Crystallization Kinetics of Mechanically Alloyed $Al_{80}Fe_{20}$ Amorphous Powder

Nguyen Thi Hoang Oanh, Tran Quoc Lap, Pham Ngoc Dieu Quynh, Le Hong Thang, Nguyen Thi Anh Nguyet, Pham Ngoc Huyen, Nguyen Hoang Viet[*]

Hanoi University of Science and Technology – No. 1, Dai Co Viet Str., Hai Ba Trung, Ha Noi, Viet Nam

Received: June 15, 2016; accepted: June 9, 2017

Abstract

The crystallization kinetics of an $Al_{80}Fe_{20}$ amorphous powder alloy were investigated by thermal analysis. Crystallization of amorphous $Al_{80}Fe_{20}$ during continuous heating undergoes four stages. The first-stage crystallization leads to the formation of fcc-Al from amorphous matrix. The next stages are the decomposition of the residual amorphous phase into several intermetallic compounds. The activation energies of the alloy were calculated from differential scanning calorimetry data using the Kissinger, Ozawa and Augis–Bennett models. The non-isothermal crystallization kinetics are analyzed by Johnson-Mehl-Avrami equation. The value of the Avrami index indicated that the crystallization is interface - controlled growth.

Keywords: amorphous alloys, mechanical alloying, crystallization kinetics, Avrami exponent

1. Introduction

Al-rich metallic glasses have generated considerable research interest because of the excellent mechanical and chemical properties. Tensile strength of Al-based amorphous alloys is 2-5 times higher than their conventional crystalline counterparts [1-3]. Their high tensile strength can be further enhanced if fcc-Al nano-particles are homogeneously dispersed within a certain size and fraction range through primary crystallization [4, 5]. One of the critical aspects of their applications is thermal stability, as the amorphous state is a non-equilibrium phase which irreversibly crystallizes upon heating. The crystallization kinetics are very important for the development of amorphous alloys and nanocrystalline materials, the properties of which are strongly affected by the crystallization process. Therefore, the crystallization kinetics of amorphous alloys have been studied extensively. Controlling the microstructure development from the glassy precursors requires detailed understanding of the specific mechanisms influencing structural transformations. Moreover, crystallization studies are essential for the proper choice of the consolidation parameters in order to maximize densification and, at the same time, retaining the desired microstructure [6, 7].

Differential scanning calorimetry (DSC) technique allows a rapid and precise determination of crystallization temperatures of amorphous materials. DSC has also led to the study of the crystallization kinetics by so-called non-isothermal methods.

Several reports on the successful formation of an amorphous phase through MA have been published for $Al_{80}Fe_{20}$ amorphous alloy [2, 8-10]. But there is a lack of studies regarding the crystallization kinetics of $Al_{80}Fe_{20}$ amorphous alloy.

In this study, the thermal stability as well as the crystallization kinetics of the mechanically alloyed $Al_{80}Fe_{20}$ amorphous powder has been investigated using DSC in non-isothermal modes. The value of the Avrami index is calculated by Johnson-Mehl-Avrami equation to determine crystallization mechanism of $Al_{80}Fe_{20}$ amorphous powder.

2. Experimental

$Al_{80}Fe_{20}$ amorphous alloy powder was prepared via mechanical alloying process after 60h of milling (more details in [11]). The structure of the as-received samples was confirmed by XRD measurements using RIGAKU RINT-2000 with CuKα (λ=1.5405Å) radiation. Morphology of the amorphous powder samples was observed by a field emission scanning electron microscope (FE-SEM). The crystallization kinetic of the powders was evaluated by non-isothermal DSC under a continuous flow of Ar gas (70 mL/min) at heating rates of 5, 10, 20 and 40 K/min using NETZSCH STA 409C, where platinum cups were used as containers.

3. Results and disscution

Fig. 1 shows the XRD pattern of $Al_{80}Fe_{20}$ powder mixture presented a fully amorphous structure after 60 hours of milling.

[*] Corresponding author: Tel.: (+84) 904.777.570
Email: viet.nguyenhoang@hust.edu.vn

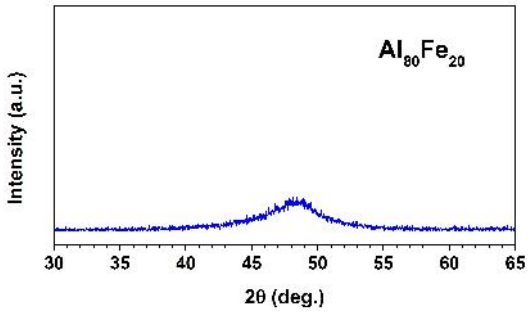

Fig. 1. X-ray diffraction patterns of $Al_{80}Fe_{20}$ amorphous powder.

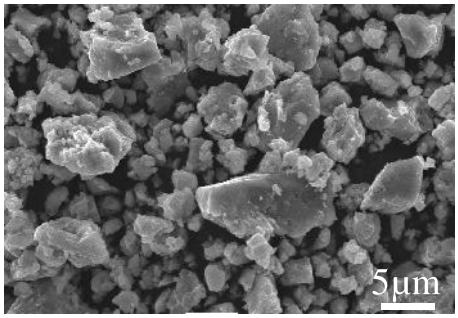

Fig. 2. FE-SEM image of $Al_{80}Fe_{20}$ amorphous powder after 60h of milling.

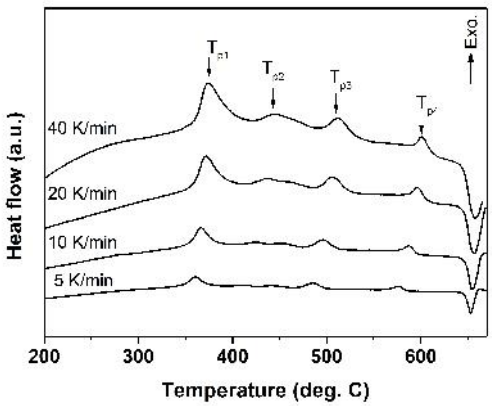

Fig. 3. DSC curves of $Al_{80}Fe_{20}$ amorphous powder at various heating rates.

Fig. 2 illustrates the SEM/EDS observation for as-received $Al_{80}Fe_{20}$ amorphous powder. It can be seen that fine powder particles, the particle size mostly below 15 μm, were agglomerated to form larger particles

Fig. 3 presents the DSC diagram for the $Al_{80}Fe_{20}$ amorphous powder as a function of temperature taken at different heating rates. As can be seen, this powder has four crystallization peaks, which means that powder undergoes four crystallization stages. Moreover, increasing the heating rate from 5 to 40 °C/min caused all position of the exothermic crystallization peaks shift to higher temperatures. The peak temperature (T_p) values at different heating rates are summarized in Table 1.

Table 1. Characteristic temperature at crystallization peaks of $Al_{80}Fe_{20}$ powder at different heating rates

Heating rate, K/min	T_{p1}, °C	T_{p2}, °C	T_{p3}, °C	T_{p4}, °C
5	360.9	412.0	486.0	576,.9
10	366.1	424.0	496.5	587.6
20	371.7	438.2	506.8	596.4
40	373.6	445.9	512.5	601.3

Similar observation for the temperature peak for the first crystallization peak of those amorphous samples were made by F. Zhou [8] with T_{p1} about 400 °C. These amorphous alloys have crystallization temperature range from 300 °C to 640 °C by F. Zhou and from 350 °C to 630 °C in this study.

The activation energy of the crystallization process gives important information regarding the thermal stability of the sample. It can be evaluated from constant-rate heating DSC curves taken at different heating rates using the Kissinger Ozawa and Augis-Bennett equations, as given by equation (1), (2), (3), respectively: [12]

$$\ln\left(\frac{\beta}{T_p^2}\right) = -\frac{E_a}{RT_p} + const \quad (1)$$

$$\ln(\beta) = -\frac{E_a}{RT_p} + const \quad (2)$$

$$\ln\left(\frac{\beta}{T_p - T_o}\right) = -\frac{E_a}{RT_p} + const \quad (3)$$

where β is the heating rate, T_p is the temperature at the exothermal peak, R is the gas constant and E_a is the activation energy of crystallization. Figure 4-6 show that Kissinger plot $\ln(\beta/T_p^2)$ versus $1000/T_p$, Ozawa plot $\ln(\beta)$ versus $1000/T_p$, Augis-Bennett plot $\ln(\beta/T_p-T_o)$ versus $1000/T_p$, which yields straight lines with a good fit, respectively. Table 2 presents results of the activation energy calculated through three methods.

Table 2. Activation energy (E_a [kJ/mol]) of $Al_{80}Fe_{20}$ amorphous powder for the crystallization stages determined via three methods

Methods	Active Energy, kJ/mol			
	Peak 1	Peak 2	Peak 3	Peak 4
Kissinger	510.1	230.2	362.6	493.2
Ozawa	520.7	241.8	375.4	507.6
Augis-Bennett	515.4	236.0	369.0	500.4

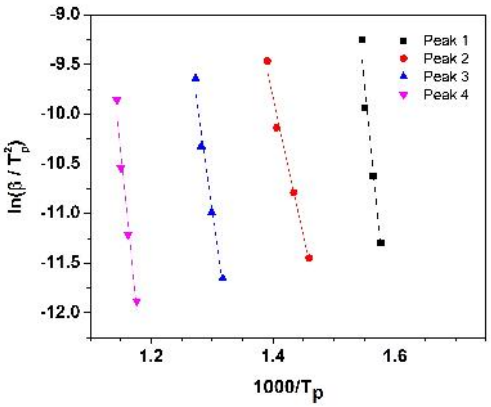

Fig. 4. Kissinger plots of the $Al_{80}Fe_{20}$ amorphous powder.

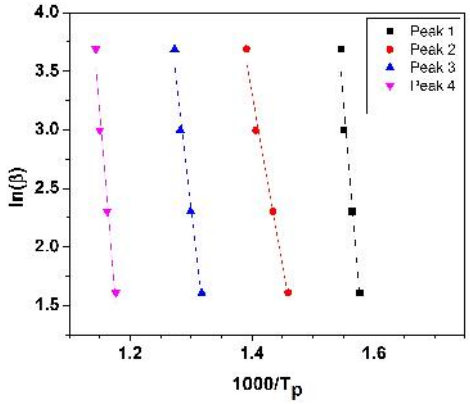

Fig. 5. Ozawa plots of the $Al_{80}Fe_{20}$ amorphous powder.

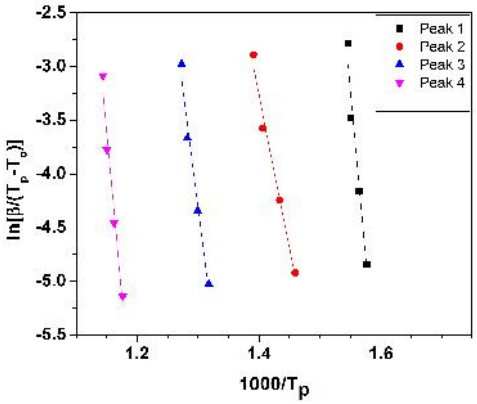

Fig. 6. Augis-Bennett plots of the $Al_{80}Fe_{20}$ amorphous powder.

It can be seen, the values of the activation energies calculated from three models are approximate. Therefore, we can use one of the three methods to calculate the activation energy.

The Avrami index (n) gives detailed information on the nucleation and growth mechanism of new crystalline grains during the phase transition, which can be obtained by Johnson-Mehl-Avrami (JMA) equation: [12]

$$x(t) = 1 - e^{-kt^n} \tag{4}$$

where x is the crystallization volume fraction at time t, n is the Avrami exponent and k is the reaction rate constant related to absolute temperature described by Arrhenius equation:

$$k = k_o \cdot e^{-\frac{E_a}{RT}} \tag{5}$$

where k_0 is a constant, E_a is the activation energy, R is the gas constant and T is the absolute temperature.

There are 2 methods to determine the Avrami parameter. The first method was proposed by Ozawa. We have:

$$\left.\frac{d\ln(-\ln(1-x))}{d\ln \ell}\right|_T = -n \tag{6}$$

The value of x at any selected T is calculated from the ratio of the partial area of the crystallization peak at the selected temperature T to the total area of the exothermic peak. Fig. 7 shows diagram of crystallized volume fraction for $Al_{80}Fe_{20}$ amorphous powder.

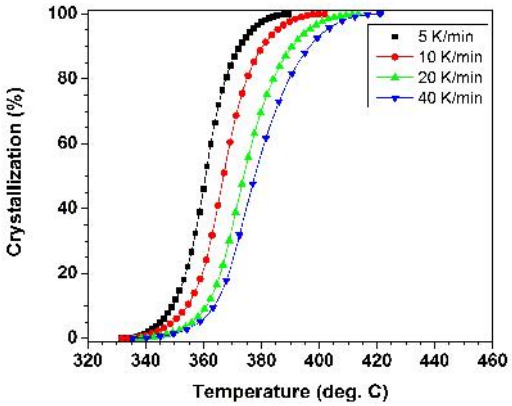

Fig. 7. Crystallized volume fraction x for $Al_{80}Fe_{20}$ powder at different heating rates.

Combining equation (6) and plot (7), at any fixed temperature, we can consider the Avrami parameter to be 0.91 in the first crystallization event.

The second method to calculate Avrami parameter is through the activation energy calculated by Kissinger method, as following

$$n(x) = -\frac{R \cdot \partial \ln(-\ln(1-x))}{E_x \cdot \partial\left(\frac{1}{T}\right)} \qquad (7)$$

The crystallized volume fraction is also determined by measuring the corresponding partial area of the exothermic peak. Plotting ln[-ln(1-x)] versus ln(1/T) with x between the range of 15% to 85% of transformed fractions, the JMA plots at different heating rates are obtained as in Fig. 8.

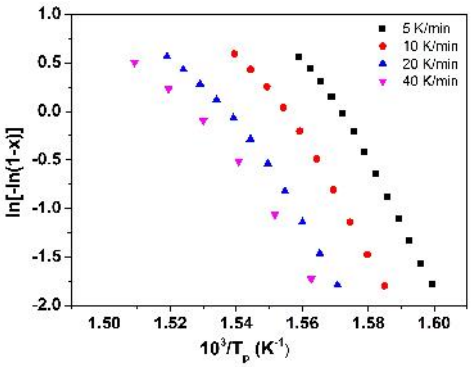

Fig. 8. JMA plots for 1st crystallization peaks of $Al_{80}Fe_{20}$ amorphous alloys at different heating rates.

The Avrami index was obtained by the slopes of these plots. The Avrami index (n) is 0.80 in the first crystallization process. According to calculated Avrami index calculated by 2 methods is approximate to 1. The Avrami index usually between 1 and 4 if the growth of the crystal is diffusion controlled. With n less than 1, the crystal growth has been shown to be interface controlled [13]. A low value of n has also been reported by other investigators in the primary crystallization of amorphous alloys. This value suggesting that the transformation in this stage is interface-controlled growth [14].

In order to determine the products of crystallization, milled powders were annealed in the DSC by heating at 20 °C/min to temperature in the range of 413 and 670 °C, coressponding to the end temperatures of four crystallization reactions. Fig. 9 shows XRD spectra from the amorphous $Al_{80}Fe_{20}$ alloy after heat treatment at different temperatures. After heating to 413 °C, the amorphous alloy began to crystallize into fcc-Al phase and remain amorphous phase. After increase heating temperature to 468 °C intermetallic phases of $Al_{13}Fe_4$, Al_3Fe and Al_6Fe can be detected from XRD pattern in Fig. 8 (b). At higher temperature of 535 °C cleary diffraction peaks of $Al_{13}Fe_4$ and Al_6Fe phases can be seen Fig. 8 (c). At the final heating temperature of 670 °C, no amorphous phase can be retained, phases of fcc-Al and $Al_{13}Fe_4$ can be obtained. Similar observation regarding products of structural changes for the amorphous alloy were made by F. Zhou et al. [8], and M. Krasnowski [2].

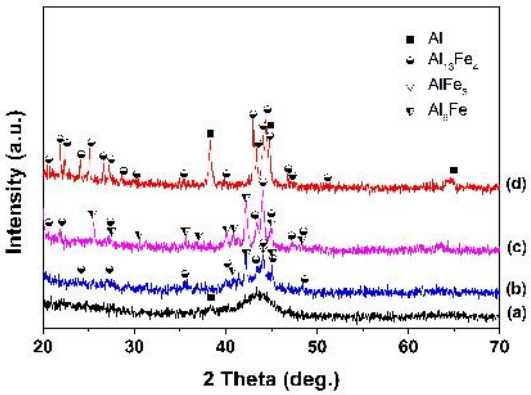

Fig. 9. XRD patterns from amorphous $Al_{80}Fe_{20}$ alloy after heat treatment at temperatures at (a) 413, (b) 468, (c) 535 and (d) 670 °C.

4. Conclusion

Crystallization kinetics of mechanically alloyed $Al_{80}Fe_{20}$ amorphous powder have been investigated using DSC in non-isothermal modes. The crystallization behavior of amorphous powder occurs in four stages in the temperature range of 350 and 630 °C. The primary phase of fcc Al together with maintaining amorphous phase in the first crystallization event followed by formation of $Al_{13}Fe_4$, Al_3Fe and Al_6Fe intermetallic phases in the second crystallization event. At the higher crystallization temperature in the third crystallization stage, intermetallic phases of $Al_{13}Fe_4$ and Al_6Fe occurred. In the final exothermic event, phases of fcc-Al, $Al_{13}Fe_4$ and $AlFe_3$ can be realized. The values of activation energy calculated from three methods Kissinger, Ozawa and Augis-Bennett are almost same. The Avrami exponent is less than 1 for the first crystallization peak, suggesting that the transformation was interface - controlled growth.

Acknowledgments

This research is funded by Vietnam National Foundation for Science and Technology Development (NAFOSTED) under grant number 103.02-2012.19.

References

[1]. John H. Perepezko and Rainer J. Hebert, Amorphous Aluminum Alloys—Synthesis and Stability. JOM, 54 (2002) 34-39.

[2]. M. Krasnowski and T. Kulik, Nanocrystalline and amorphous Al-Fe alloys containing 60-85% of Al synthesised by mechanical alloying and phase transformations induced by heating of

milling products. Materials Chemistry and Physics, 116 (2009) 631-637.

[3]. Akihisa Inoue, Amorphous, nanoquasicrystalline and nanocrystalline alloys in Al-based systems. Progress in Materials Science, 43 (1998) 365-520.

[4]. Sergio Scudino, Kumar B. Surreddi, Hoang V. Nguyen, Gang Liu, Thomas Gemming, Mira Sakaliyska, Ji S. Kim, Jens Vierke, Markus Wollgarten, and Jurgen Eckert, High-strength $Al_{87}Ni_8La_5$ bulk alloy produced by spark plasma sintering of gas atomized powders. Journal of Materials Research, 24 (2009) 2909-2916.

[5]. Akihisa Inoue and Hisamichi Kimura, High-strength Al-based nanostructure alloys. Current Opinion in Solid State and Materials Science, 2 (1997) 305-310.

[6]. P. P. Choi, J. S. Kim, O. T. H. Nguyen, D. H. Kwon, Y. S. Kwon, and J. C. Kim, Al-La-Ni-Fe bulk metallic glasses produced by mechanical alloying and spark-plasma sintering. Materials Science and Engineering: A, 449-451 (2007) 1119-1122.

[7]. K. B. Surreddi, S. Scudino, M. Sakaliyska, K. G. Prashanth, D. J. Sordelet, and J. Eckert, Crystallization behavior and consolidation of gas-atomized $Al_{84}Gd_6Ni_7Co_3$ glassy powder. Journal of Alloys and Compounds, 491 (2010) 137-142.

[8]. F. Zhou, R. Lück, M. Scheffer, D. Lang, and K. Lu, The crystallization process of amorphous $Al_{80}Fe_{20}$ alloy powders prepared by ball milling. Journal of Non-Crystalline Solids, 250–252, Part 2 (1999) 704-708.

[9]. J. Noetzel, D.C. Meyer, A. Tselev, A. Mücklich, P. Paufler, F. Prokert, E. Wieser, and W. Möller, Amorphization of Fe/Al: bulk and thin-film effects. Applied Physics A, 71 (2000) 47-54.

[10]. Wang Genmiao, Zhang Daoyuan, Chen Huiyu, Lin Bixia, Wang Weihua, and Dong Yuanda, Formation and properties of $Fe_{20}Al_{80}$ amorphous powder. Physics Letters A, 155 (1991) 57-61.

[11]. Nguyen Hoang Viet, Nguyen Thi Hoang Oanh, Pham Ngoc Dieu Quynh, Tran Quoc Lap, and Kim Ji Soon. Bulk Amorphous $Al_{80}Fe_{20}$ Produced by Mechanical Alloying and Spark-Plasma Sintering. in *The 2nd International Conference on Advanced Materials and Nanotechnology* 2014. Hanoi: Bach Khoa Publishing house.

[12]. Miray Çelikbilek, Ali Erçin Ersundu, and Süheyla Aydın, Chapter 6 - Crystallization Kinetics of Amorphous Materials, in Advances in Crystallization Processes, Y. Mastai, Editor. 2012, InTech. p. 127-158.

[13]. S. W. Du and R. V. Ramanujan, Crystallization and magnetic properties of $Fe_{40}Ni_{38}B_{18}Mo_4$ amorphous alloy. Journal of Non-Crystalline Solids, 351 (2005) 3105-3113.

[14]. J.W. Christian, *The Theory of Transformations in Metals and Alloys*. 1975, Netherlands: Pergamon, Oxford.